Ceramics International 44 (2018) 14896–14900

Contents lists available at ScienceDirect

Ceramics International

journal homepage: www.elsevier.com/locate/ceramint

Short communication

Crystal structure and wave-transparent properties of lithium aluminum silicate glass-ceramics

Long Xia[a], Yanan Yang[a], Xinyu Zhang[a], Jian Zhang[a], Bo Zhong[a], Tao Zhang[a,*], Huatao Wang[a], Guangwu Wen[b]

[a] School of Materials Science and Engineering, Harbin Institute of Technology (Weihai), Weihai 264209, PR China
[b] School of Materials Science and Engineering, Shandong University of Technology, Zibo 255049, PR China

ARTICLE INFO

Keywords:
Glass-ceramics
β-spodumene
Crystallization
Microwave transmittance
Polarization loss

ABSTRACT

Lithium aluminum silicate (LAS) glass-ceramic exhibits high transmittance to electromagnetic wave and is an ideal radome material. LAS glass-ceramics with different ratios of Li/Al were prepared by sol-gel method. Crystallization behaviors and wave-transparent properties of sintered powders were characterized. *β*-spodumene was detected as the major phase that precipitated from the sample with 1:1 ratio between Li and Al, which exhibited ultra-low complex permittivity (epsilon, 2.78) and dielectric loss tangent values. The microwave transmittance in 2–18 GHz is higher than 90% when the thickness is within 1.7 mm, suggesting that this kind of LAS glass-ceramic possesses excellent wave-transparent properties.

1. Introduction

With the rapid development of electromagnetic (EM) wave circuit devices and information technology, wave-transparent materials are urgently demanded in many areas, such as mobile phone, antenna and radome [1–4]. In order to ensure a low energy consumption, wave-transparent materials must possess two important parameters, low permittivity ε and low dielectric loss tangent tanδ. In general, in the frequency range from 0.3 GHz to 300 GHz, to obtain ideal materials with wave-transparent and much low loss performance, the ε value of wave-transparent materials should be among 1–4, and the value of tanδ is in the order of 10^{-3} to 10^{-2} [5].

Glass-ceramic is a kind of polycrystalline solid material containing a large quantity of microcrystalline phases and amorphous phases, which is obtained by controlling crystallization behaviors through heat treatment [6]. Glass-ceramic has been extensively investigated and widely used in the fields of aerospace, anti-corrosion materials, high temperature stable materials, wear-resistant materials and optical instruments [7,8]. LAS glass-ceramic is an important role of glass-ceramics systems and famous for its high temperature stability, thermal shock resistance and ultra-low or even negative thermal expansion coefficient [9,10]. At the same time, LAS exhibits excellent wave-transparent properties. LAS glass-ceramics can be divided into two main categories according to main crystal phase: eucryptite and spodumene solid solution. Besides, *β*-spodumene can be regarded as the most stable crystalline phase at high temperature, and dielectric loss of spodumene is lower than eucryptite [11,12]. To the best of our knowledge, however, there is little literature on wave-transparent of spodumene. Therefore, this work focuses on the study of wave-transparent properties of LAS glass-ceramics with different ratios of Li/Al.

2. Experimental

LAS gel precursor powders were synthesized through sol-gel method by hydrolysis of inorganic salts according to our previous work [13]. The schematic flow chart is given in Fig. 1. Gel powders with different molar ratios of Li/Al were prepared from silica sol, $Al(NO_3)_3{\cdot}9H_2O$ and $LiNO_3$.

Firstly, $Al(NO_3)_3{\cdot}9H_2O$ was dissolved in an aqueous solution at 75 °C. Ammonia water was dripped and stirred to promote hydrolysis to form a boehmite (γ-AlOOH) sol. To prepare the lithium-aluminum sol with different mole ratios of Li/Al, $LiNO_3$ solution was added into the boehmite sol with a series of mole ratios between lithium and aluminum including 0.6: 1.4, 0.8: 1.2, 1: 1, 1.2: 0.8 and 1.4: 0.6, and then the mixture was stirred until a lithium-aluminum sol was formed. Silica sol was slowly added to the lithium-aluminum sol, and LAS sol was acquired after stirring at 75 °C for 3–4 h. Finally, the LAS sol was dried at 100 °C to obtain LAS gel precursor powders. LAS glass-ceramics with different ratios prepared as described above are designated as Li0.6Al1.4, Li0.8Al1.2, Li1Al1, Li1.2Al0.8 and Li1.4Al0.6, respectively.

* Corresponding author.
E-mail address: xialonghit@gmail.com (T. Zhang).

https://doi.org/10.1016/j.ceramint.2018.04.202
Received 14 December 2017; Received in revised form 20 March 2018; Accepted 23 April 2018
Available online 25 April 2018

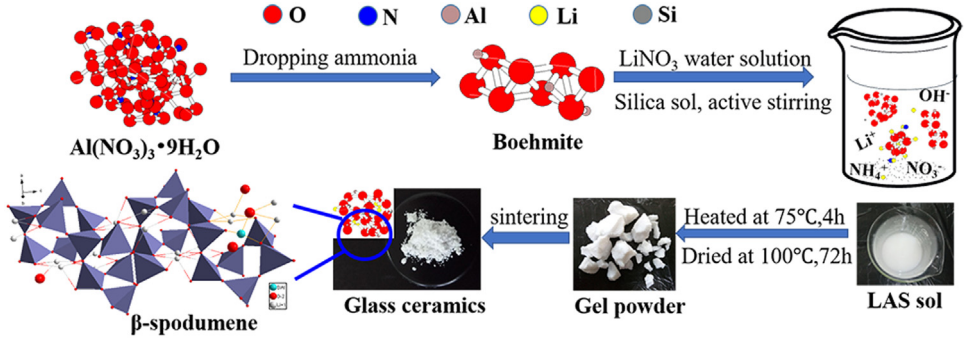

Fig. 1. Schematic diagram of preparing LAS gel.

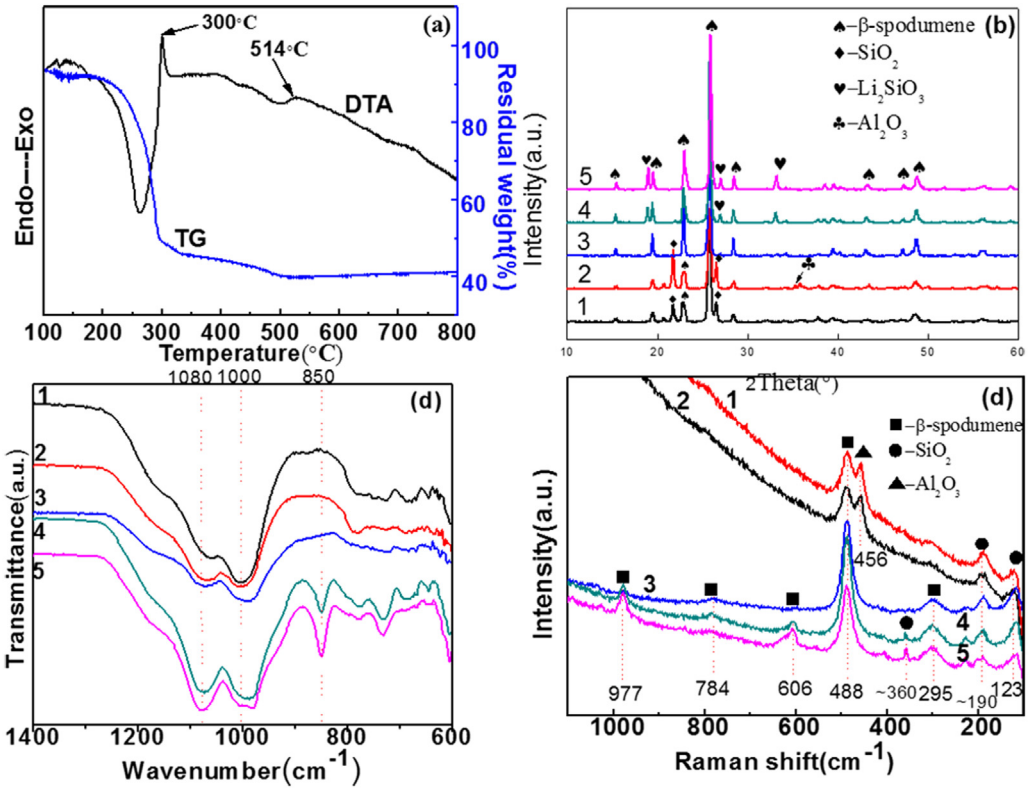

Fig. 2. (a) TG-DTA curves of LAS gel, (b) XRD patterns, (c) FT-IR spectra, (d) Raman spectra of sintered LAS powders with different molar ratios. Sample 1, 2, 3, 4 and 5 represent Li0.6Al1.4, Li0.8Al1.2, Li1Al1, Li1.2Al0.8 and Li1.4Al0.6, respectively.

3. Results and discussion

The thermogravimetry (TG) and differential thermal analysis (DTA) curves of Li0.6Al1.4 are shown in Fig. 2a. A significant endothermic peak is observed in DTA curve at about 300 °C, corresponding to a significant weight loss in TG curve, which is mainly caused by the removal of bound water and decomposition of nitrate in the gel. When temperature increases to 500 °C, the quality of gel powders gradually becomes stable, indicating that nitrate decomposes slowly at this stage [14]. The endothermic peak at 514 °C in DTA curve corresponds to precipitation of *β*-spodumene.

Combined with TG-DTA test results, the heat treatment process of LAS is as follows. Initially, LAS gel precursor powders were heated up to 200 °C and held for 12 h to remove water molecules, then, pyrolyzed at 500 °C for 1 h to decompose nitrate. Finally, gel powders were heated at 1200 °C in the air for 1 h, then cooled down to room temperature naturally.

The X-ray diffraction (XRD) patterns of gel powders with different ratios are shown in Fig. 2b. The main crystalline phase of Li0.6Al1.4 and Li0.8Al1.2 is *β*-spodumene, whose lattice parameters are 7.539 Å × 7.539 Å × 9.149 Å, and silica and Al_2O_3 are also observed. *β*-spodumene phase is the only crystalline phase precipitated in Li1Al1. In addition to *β*-spodumene, Li_2SiO_3 is also detected in Li1.2Al0.8 and Li1.4Al0.6.

In order to study structural changes of LAS with different compositions, Fourier transform infrared spectroscopy (FTIR) studies are performed in the wavenumber range 4000–600 cm^{-1}. However, the spectra in the wavenumber region 1300–600 cm^{-1} are presented in Fig. 2c. Fig. 2c illustrates that a strong broad band in the wavenumber region 1100–1000 cm^{-1} appears in all samples. Two strong absorption bands at around 1080 cm^{-1} and 1000 cm^{-1} appear corresponding to the asymmetric characteristic vibration of Si-O-Si and the symmetrical stretching vibration of Si-O-Al [15], respectively, suggesting the replacement for SiO_4 tetrahedron with AlO_4 tetrahedron. With the increase in the ratio of Li/Al, 1080 cm^{-1} peak becomes sharp, representing that more quartz phase precipitates. A medium strong band at around 850 cm^{-1} is found in Li1.2Al0.8 and Li1.4Al0.6, due to the characteristic vibration of AlO_6 octahedron with non-bridging oxygens

[16]. Conversely, such band is not observed in Li0.6Al1.4, Li0.8Al1.2 and Li1Al1, suggesting that part of AlO_6 octahedrons change into AlO_4 tetrahedrons. The residual AlO_6 octahedrons are not joined into the network of LAS glass. Consequently, the homogeneity of LAS is weakened [17]. A strong absorption band in the region 720–780 cm^{-1} appears in all samples, indicating the characteristic vibration of Al-O covalent bond in AlO_4 tetrahedron in β-spodumene [16]. The above FTIR results corroborate the crystallization results obtained from XRD.

The Raman spectra of heat-treated glass-ceramics with different proportions of components are shown in Fig. 2d. An intensive band at 456 cm^{-1} appears both in Li0.6Al1.4 and Li0.8Al1.2. With the increase in proportion of Li/Al, the weak bands arise at 300, 360, 606, 784 and 977 cm^{-1}. The peaks at 488 cm^{-1} and 784 cm^{-1} correspond to the vibrations of Si-O bonds in SiO_4 tetrahedrons in the network structure. Frequency and intensity of the peak at 488 cm^{-1} depend on the bond angle and the non-bridging oxygen number of the Si-O-Si bond. The Raman peak at 784 cm^{-1} belongs to the non-uniform vibration of SiO_4 tetrahedrons [18]. Intensity and frequency of the peak are determined by the degree of connection of glass network structure and the non-bridging oxygen number. The above Raman results corroborate the crystallization results obtained from XRD. Just as the crystallization behaviors of Li0.6Al1.4 and Li0.8Al1.2 are consistent, the behaviors of Li1.2Al0.8 and Li1.4Al0.6 are the same. So, Li0.6Al1.4 and Li1.4Al0.6 are selected as representatives of the change in ratios of Li/Al for analysis of scanning electron microscopy (SEM) and microwave absorption properties test.

Microstructural features of LAS powders with different ratios are shown in Fig. 3. The morphology of sintered gel powders demonstrates polygonal shape with the size of 1–2 μm. The overviews of surface morphology of LAS powders are illustrated in Fig. 3a, b, and c and the corresponding detailed characterizations of LAS powders are displayed in Fig. 3d, e and f, respectively. It can be observed that the microstructure of crystal surface shows the lamellar microstructure. There is no obvious difference in the morphology and the size of the smallest powder with different proportions.

The complex permittivity ($\varepsilon_r = \varepsilon' - j\varepsilon''$) values of LAS with different ratios are shown in Fig. 4. As can be seen from the Fig. 4a, with the change of ratios, the real permittivity (ε') increases and the variation range becomes larger. It should be noticed that both of variation range and real permittivity of Li1Al1 are the smallest (ε' is about 2.8). Similarly, the imaginary part (ε'') of the complex permittivity shows an unstable trend and the variation range increases (Fig. 4b) as the ratio changes. The imaginary part of the complex permittivity indicates the ability to dissipate EM wave [19], and the imaginary permittivity of Li1Al1 has the smallest value, indicating that dielectric loss is small. As shown in Fig. 4c, Li1All exhibits the best wave-transparent performance compared with other samples for the reason that the dielectric loss tangent ($\tan\delta_\varepsilon = \varepsilon''/\varepsilon'$) is close to zero. In addition, the bandwidth of the dielectric loss tangent of Li1Al1 less than 0.01 can reach up to 5 GHz (from 2 GHz to 7 GHz).

To better illustrate microwave transmittance of LAS, computer simulation has been given and the results are shown in Fig. 5. On the basis of single-layer composite wave-transparent principle, the three-dimensional relations between microwave transmittance, frequency and thickness of samples can be calculated by Eqs. (1)–(4).

$$R = \frac{1-n}{1+n} \tag{1}$$

$$n = \frac{\varepsilon_r \cos\theta}{(\varepsilon_r - \sin^2\theta)^{1/2}} \tag{2}$$

$$|T^2| = \frac{(1-R^2)}{(1-R^2)+4R^2\sin^2\varphi} \tag{3}$$

$$\varphi = \frac{2\pi d}{\lambda}(\varepsilon_r - \sin^2\theta)^{1/2} \tag{4}$$

where R is the reflection coefficient, n is the EM wave refractive index, T is the microwave transmittance, ε_r is the relative complex permittivity, d is the thickness of the sample, λ is the EM wave length and θ is the incident angle of EM wave. For the vertical incident of waves, $\theta = 0$.

It is observed that the microwave transmittance of LAS glass-ceramics varies with thickness and frequency. To obtain a more accessible representation of transmittance, the planar projections of transmittance of Li0.6Al1.4, Li1.4Al0.6 and Li1Al1 are shown in Fig. 5d, e and f, respectively. The transmittance of Li1Al1 is compared with paraffin used in the test. It can be seen from the Fig. 5a and b that the transmittance of Li1Al1 is more than 86.9%, while the transmittance of paraffin is 91.5% or more, with the thicknesses varying from 1 to 10 mm in the range 2–18 GHz, which indicates that the wave-transparent of Li1Al1 is similar to paraffin. It can be seen from Fig. 5d, e and f that the change in

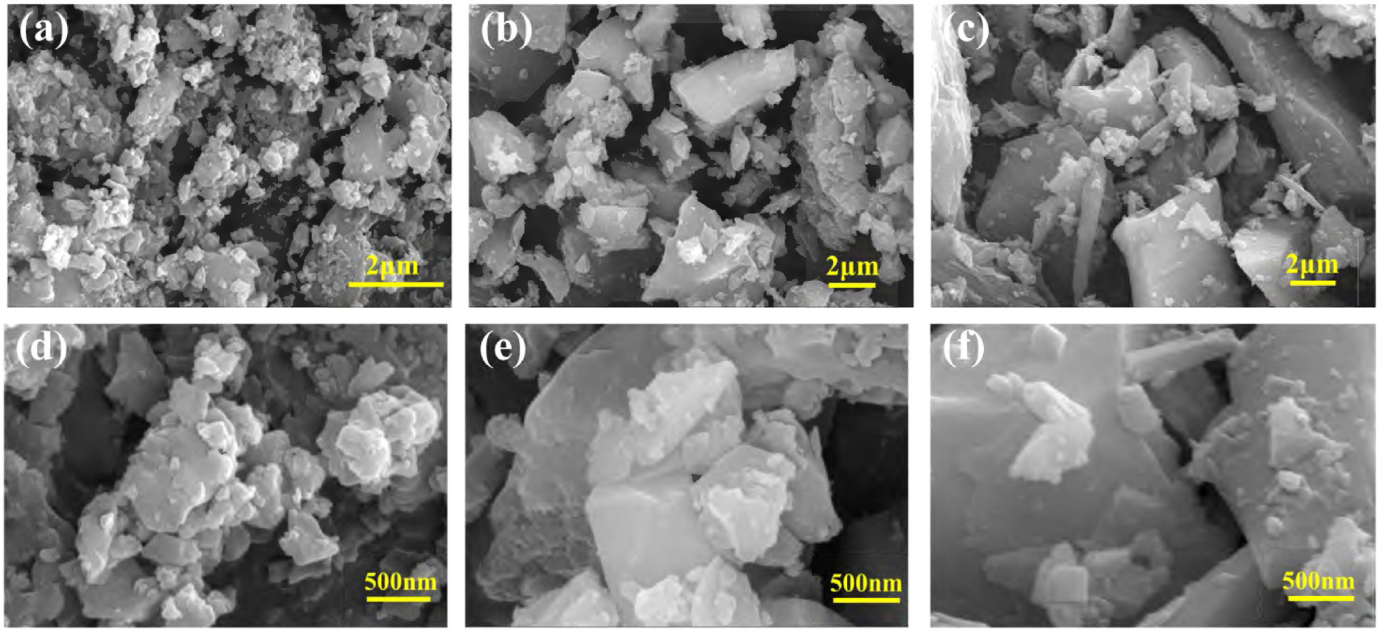

Fig. 3. SEM photographs of the LAS powders calcined at 1200 °C for 1 h. (a, d) Li0.6Al1.4, (b, e) Li1Al1, (c, f) Li1.4Al0.6.

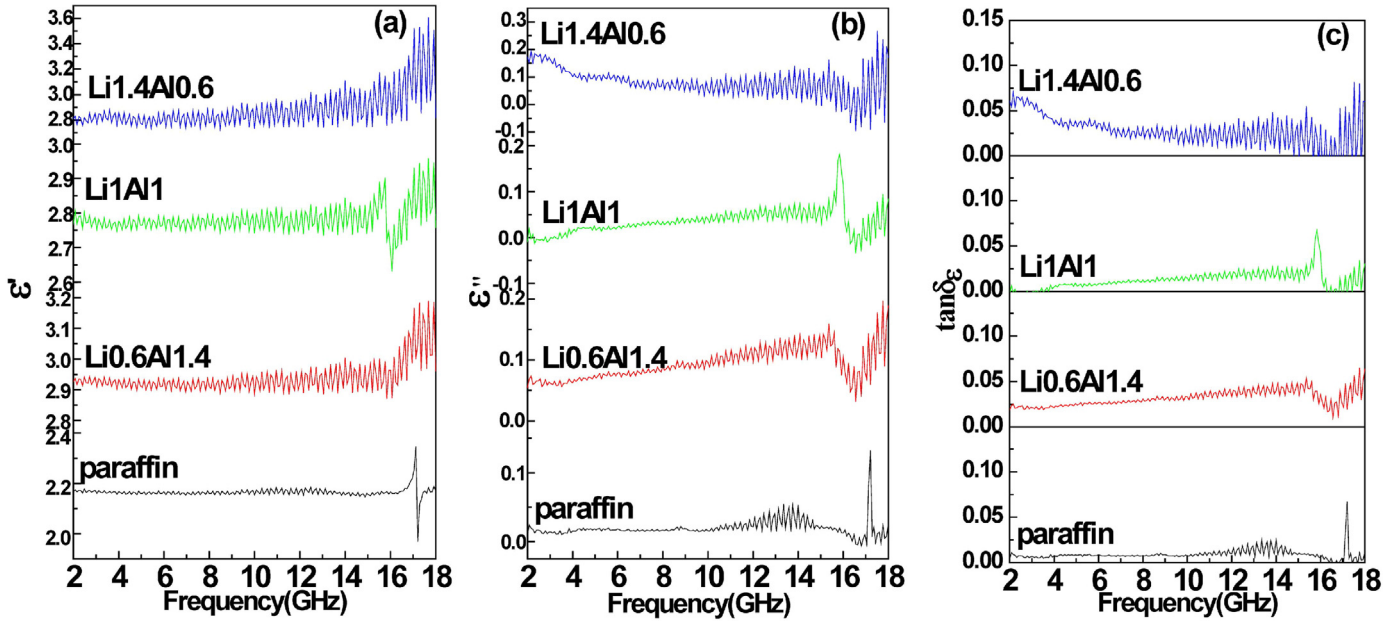

Fig. 4. Wave-transparent performance of LAS powders with different proportions: (a) real part of relative complex permittivity, (b) imaginary part of relative complex permittivity, (c) dielectric loss tangent.

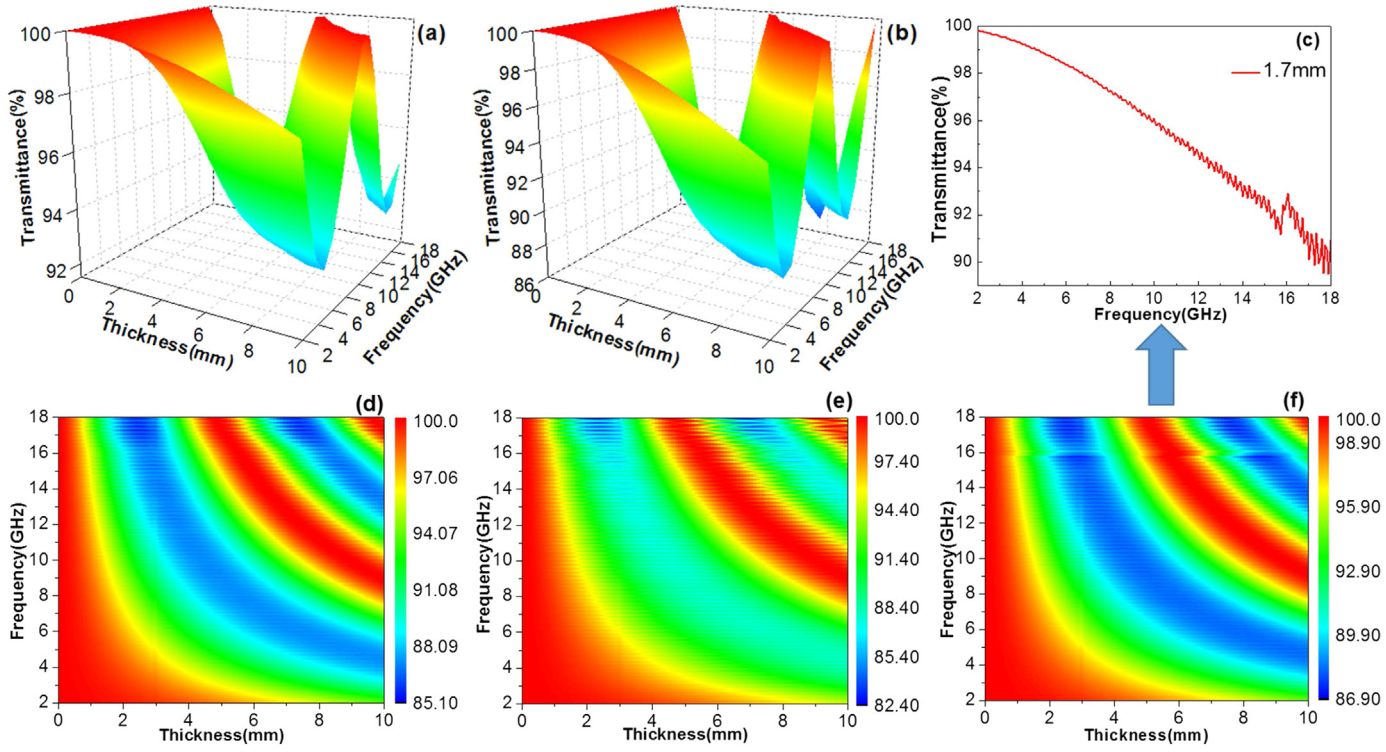

Fig. 5. Microwave transmittance of (a) paraffin, (b) Li1Al1, (c) Li1Al1 at 1.7 mm, testing under room temperature. Plane projection map of microwave transmittance: (d) Li0.6Al1.4, (e) Li1.4Al0.6 (f) Li1Al1.

the ratio of Li/Al has an adverse effect on the wave-transparent performance, because the minimum microwave transmittances of Li0.6Al1.4 and Li1.4Al0.6 are reduced to 85.1% and 82.4%, respectively. The transmittance of Li1Al1 in the entire frequency band at 1.7 mm is shown in Fig. 5c. The microwave transmittance is higher than 90% in the range 2–18 GHz when the thickness is within 1.7 mm, demonstrating that it has an extensive application as the surface wave-transparent layer of EM absorbing materials. Chen et al. reported the successful preparation of in-situ mullite whiskers reinforced aluminum chromium phosphate wave-transparent ceramics, and they found that all transmittances are greater than 60% as the thickness varies from 5 mm to 15 mm, and especially greater than 80% with the value of 7 mm [20]. Sebastian et al. reported low loss dielectric materials for low temperature cofired ceramic (LTCC) [21]. According to the article, most glass-ceramics have a dielectric constant of 5–10, for example, the ε_r of Li_2O-B_2O_3-SiO_2 (35.4: 31.66: 33.2) is 6.44. Compared with these reported glass ceramics, LAS glass-ceramics indicate excellent electromagnetic wave transmission regardless of microwave transmittance or

dielectric constant.

The crystal structure of β-spodumene is simulated based on comprehensive analyses of XRD, FTIR and Raman results, as shown in Fig. 1. β-spodumene belongs to the tetragonal system, where tetrahedrons are connected to form a network space structure. Some of the silicon atoms are replaced by aluminum atoms and voids are formed in this structure. Lithium ions are filled in network gaps to maintain the electrical neutrality. The tetrahedrons composed of Si-O and Al-O form the five-membered ring structure in the space, which is a basic unit of spiral chains of the integrated crystal structure. Lithium ion is coordinated with the surrounding four oxygen atoms in the channel with a diameter of 3 Å at c-axis direction [22].

From the view of phase composition, the glass-ceramic is composed of crystal phases and amorphous phases, and the energy loss is mainly from conductance losses, relaxation polarization losses and structural losses. Under the action of external electric field, only electronic or ionic elastic displacement polarization exists and electronic and ionic elastic displacement polarization basically do not consume energy. In a close structure of LAS crystals, the lithium ion is expected to be coordinated by such SiO_4/AlO_4 tetrahedral ligands [23]. Consequently, there is no polarization loss and the only slight loss is the leakage conductance loss caused by incompletely ideal media. As is known from the XRD (Fig. 2b) results, apart from β-spodumene, Al_2O_3, SiO_2 and Li_2SiO_3 also precipitate from Li0.6Al1.4 and Li1.4Al0.6. Therefore, the microstructure of resultant is loose. The loose structure causes large gaps in ionic crystals, which are easy to form thermal ionic relaxation, resulting in leakage conductance losses and polarization losses. In addition, silica and β-spodumene form a solid solution $LiAlSi_3O_8$, and the lattice distortion of solid solution could lead to the greater dielectric loss. Meanwhile, after the addition of alkali metal oxide in glass-ceramics, dielectric loss is greatly enhanced. The reason is that the greater the content of alkaline oxide is, the looser the glass structure is. As a result, ions can move easily, which produces leakage conductance losses and relaxation losses. Sample Li1.4Al0.6 contains lithium oxide, resulting in an increase in loss tangent and poorer wave-transparent performance.

4. Conclusion

In summary, the existence of β-spodumene phase in LAS glass-ceramics shows excellent wave-transparent performance. The microwave transmittance of β-spodumene is higher than 90% in the range from 2 to 18 GHz. Therefore, it is an ideal broadband wave-transparent material for radome applications. Pure β-spodumene has the lowest dielectric loss tangent and a stable dielectric constant (about 2.8). With the change of the ratio between lithium and aluminum, other crystalline phases will exist in glass-ceramics, which can increase dielectric loss and deteriorate the wave-transparent and need to be further studied. The data mentioned in the article is accurate and repeatable.

Acknowledgments

This work was supported by the Taishan Scholar Project (No. ts201511080), National Natural Science Foundation of China (Grant No. 51672059, 51172050, 51102060, 51302050), the Natural Scientific Research Innovation Foundation in Harbin Institute of Technology (HIT.NSRIF.2014129).

References

[1] M.-S. Cao, W.-L. Song, Z.-L. Hou, B. Wen, J. Yuan, The effects of temperature and frequency on the dielectric properties, electromagnetic interference shielding and microwave-absorption of short carbon fiber/silica composites, Carbon 48 (3) (2010) 788–796.
[2] J. Zheng, Z. Yu, G. Ji, X. Lin, H. Lv, Y. Du, Reduction synthesis of FexOy@SiO_2 core-shell nanostructure with enhanced microwave-absorption properties, J. Alloy. Compd. 602 (2014) 8–15.
[3] C.-H. Peng, P. Shiu Chen, C.-C. Chang, High-temperature microwave bilayer absorber based on lithium aluminum silicate/lithium aluminum silicate-SiC composite, Ceram. Int. 40 (1) (2014) 47–55.
[4] X. Yin, L. Kong, L. Zhang, L. Cheng, N. Travitzky, P. Greil, Electromagnetic properties of Si-C-N based ceramics and composites, Int. Mater. Rev. 59 (6) (2014) 326–355.
[5] Z.S. Hu, H.R. Geng, X.Q. Hou, J.F. Leng, Effect of Si_3N_4 on properties of aluminum borate whisker/aluminum phosphates ceramic, Key Eng. Mater. 575–576 (2014) 50–53.
[6] V.S. Raghuwanshi, C. Rüssel, A. Hoell, Crystallization of $ZrTiO_4$ nanocrystals in lithium-alumino-silicate glass ceramics: anomalous small-angle X-ray scattering investigation, Cryst. Growth Des. 14 (6) (2014) 2838–2845.
[7] M. Guedes, A.C. Ferro, J.M.F. Ferreira, Nucleation and crystal growth in commercial LAS compositions, J. Eur. Ceram. Soc. 21 (9) (2001) 1187–1194.
[8] V.O. Soares, O. Peitl, E.D. Zanotto, L. Pinckney, New sintered Li_2O-Al_2O_3-SiO_2 ultra-low expansion glass-ceramic, J. Am. Ceram. Soc. 96 (4) (2013) 1143–1149.
[9] Z. Qing, B. Li, H. Li, Y. Li, S. Zhang, Effects of MgO on properties of Li_2O-Al_2O_3-SiO_2 glass-ceramics for LTCC applications, J. Mater. Sci. -Mater. Electron. 25 (5) (2014) 2149–2154.
[10] F.A. Hummel, Thermal expansion properties of some synthetic lithia minerals, J. Am. Ceram. Soc. 34 (2006) 235–239.
[11] A. Ananthanarayanan, A. Dixit, R.K. Lenka, R.D. Purohit, V.K. Shrikhande, G.P. Kothiyal, Some studies on the phase formation and kinetics in TiO_2 containing lithium aluminum silicate glasses nucleated by P_2O_5, J. Therm. Anal. Calorim. 106 (3) (2011) 839–844.
[12] Q. Zhang, Y. Zhu, Z. Li, Performance investigation of Li_2O-$Al_2O_3-4SiO_2$ based glass-ceramics with B_2O_3, Na_3AlF_6 and Na_2O fluxes, J. Non-Cryst. Solids 358 (3) (2012) 680–686.
[13] L. Xia, G. Wen, L. Song, X. Wang, Sol-gel synthesis and crystallization behaviour of β-spodumene, J. Sol.-Gel Sci. Technol. 52 (1) (2009) 134–139.
[14] M.K. Naskar, M. Chatterjee, N.S. Lakshmi, Sol-emulsion-gel synthesis of hollow mullite microspheres, J. Mater. Sci. 37 (2002) 343–348.
[15] M.K. Murthy, E.M. Kirby, Infrared study of compounds and solid solutions in the system lithia-alumina-silica, J. Am. Ceram. Soc. 45 (7) (1962) 324–329.
[16] M. Chatterjee, M.K. Naskar, Sol-gel synthesis of lithium aluminum silicate powders: the effect of silica source, Ceram. Int. 32 (6) (2006) 623–632.
[17] U. Selvaraj, S. Komarneni, R. Roy, Synthesis of glass-like cordierite from metal alkoxides and characterization by ^{27}Al and ^{29}Si MASNMR, J. Am. Ceram. Soc. 73 (12) (1990) 3663–3669.
[18] I. Alekseeva, O. Dymshits, V. Ermakov, A. Zhilin, V. Petrov, M. Tsenter, Raman spectroscopy quantifying the composition of stuffed β-quartz derivative phases in lithium aluminosilicate glass-ceramics, J. Non-Cryst. Solids 354 (45–46) (2008) 4932–4939.
[19] B. Zhao, G. Shao, B. Fan, W. Guo, Y. Chen, R. Zhang, Preparation of SnO_2-coated Ni microsphere composites with controlled microwave absorption properties, Appl. Surf. Sci. 332 (2015) 112–120.
[20] N. Chen, H. Wang, J. Huo, S. Liu, J. He, Preparation and properties of in-situ mullite whiskers reinforced aluminum chromium phosphate wave-transparent ceramics, J. Eur. Ceram. Soc. 37 (2017) 4793–4799.
[21] M.T. Sebastian, H. Jantunen, Low loss dielectric materials for LTCC applications: a review, Int. Mater. Rev. 53 (2008) 57–90.
[22] W. Höland, G.H. Beall, Glass-ceramic Technology, second ed., Wiley-Blackwell, 2012.
[23] M.S. Rao, C.S. Rao, B.V. Raghavaiah, G.S. Baskaran, V. Ravikumar, I.V. Kityk, N. Veeraiah, The role of ligand coordination on the spectral features of Yb^{3+} ions in lead aluminum silicate glasses, J. Mol. Struct. 1007 (2012) 185–190.